Journal of Advanced Ceramics
2015, **4**(4): 292–299
DOI: 10.1007/s40145-015-0163-z

ISSN 2226-4108
CN 10-1154/TQ

Research Article

Rare earth (La) and metal ion (Pb) substitution induced structural and multiferroic properties of bismuth ferrite

Poorva SHARMA[a], Ashwini KUMAR[a,b], Dinesh VARSHNEY[a,*]

[a]*Materials Science Laboratory*, *School of Physics*, *Vigyan Bhawan*, *Devi Ahilya University*, *Khandwa Road Campus*, *Indore 452001*, *India*
[b]*Department of Physics*, *Southeast University*, *Jiangning District*, *Nanjing 211189*, *China*

Received: April 16, 2015; Revised: July 10, 2015; Accepted: July 14, 2015

Abstract: In this study, bulk samples of multiferroic with compositional formula, $BiFeO_3$ and $Bi_{0.825}A_{0.175}FeO_3$ (A = La, Pb), were synthesized by solid state reaction route. X-ray diffraction (XRD) along with the Rietveld refinement revealed the distorted rhombohedral ($R3c$) structure for pristine $BiFeO_3$ and $Bi_{0.825}La_{0.175}FeO_3$ and tetragonal ($P4/mmm$) for $Bi_{0.825}Pb_{0.175}FeO_3$ ceramic. To support the structural results, bond length between atoms for both of the compounds was calculated. A change in Raman mode position in $BiFeO_3$ (BFO) has been observed with La and Pb substitution from Raman scattering measurements and also recommended a structural change with rare earth and metal ion substitution at Bi site. From the frequency dependent dielectric constant and dielectric loss plots, a decrease in dielectric values with increase in frequency was observed for both of the samples. For microelectronic devices, porous ceramics with lower value of dielectric constant are most useful. Thus, further studies are also needed to carefully tune the magnetoelectric properties and structural distortion after La/Pb substitution in BFO.

Keywords: ceramics; X-ray diffraction (XRD); Raman spectroscopy; dielectric properties

1 Introduction

Multifunctional $BiFeO_3$ (BFO) materials have placed their importance in multifunctional devices, spintronics, and magnetic memory devices [1,2]. BFO has a rhombohedrally distorted perovskite structure (space group $R3c$) with high Curie temperature ($T_C \approx 1100$ K) and antiferromagnetic Néel temperature ($T_N = 675$ K) with a spatially modulated spiral spin structure [3–5]. The literature witnesses that the A-site substitution in BFO has been suggested as the most effective way to reduce the impurity phases and enhance magnetoelectric coupling constant by creating the lattice strain due to the ionic size mismatch between hosts and substituting cations [6–10]. Besides this, a structural phase evolution along with improved ferroelectric and ferromagnetic properties is noticed.

Recently, the rare earth (La) doped $BiFeO_3$ as $Bi_{0.7}La_{0.3}FeO_3$ witnesses a structural phase transition (rhombohedral→orthorhombic) with enhanced magnetoelectric interaction [11]. The rare earth (Nd) doped BFO as $Bi_{1-x}Nd_xFeO_3$ ($x = 0.05$–0.15) also documents structural evolution but from rhombohedral to triclinic structure. The magneto–electric coupling is also shown in $Bi_{1-x}Nd_xFeO_3$ near the Néel temperature ($T_N = 653$ K). However, higher Nd doping ($x = 0.175$–0.2) shows a pseudotetragonal structure [12].

* Corresponding author.
E-mail: vdinesh33@rediffmail.com

The structural phase transition is sensitive to synthesis process as rapid liquid phase sintering method. A rhombohedral to monoclinic structure for $Bi_{1-x}Nd_xFeO_3$ ($x = 0$–0.15) is thus noticed [13,14].

The rare earth (Gd) doped $Bi_{1-x}Gd_xFeO_3$ shows structural phase transition for $x = 0.1$ ($R3c \rightarrow Pn2_1a$) and for $0.2 < x < 0.3$ ($Pn2_1a \rightarrow Pnma$) with improved multiferroic property of $BiFeO_3$ [15]. At the same time, another author found that the origin of the improved magnetic and electrical properties is attributed to a possible suppression of the inhomogeneous magnetic spin structure and/or broken periodicity of the spin cycloid of BFO due to smaller crystallite size and a decrease of the oxygen vacancies, and explained that the rise in DC electrical resistivity with Gd doping in BFO is due to a variable range hopping conduction mechanism [16]. It is also noted that the room temperature X-ray diffraction patterns document both rhombohedral and triclinic structures of $Bi_{1-x}Pr_xFeO_3$ ($0 \leqslant x \leqslant 0.15$). With an increase in Pr content, the dielectric constant increases whereas the dielectric loss decreases [17]. Furthermore, the magnetic ordering is enhanced with the effective magnetic moment of the Dy ion concentration in $Bi_{0.8}Dy_{0.2-x}La_xFeO_3$ [18].

Ho substitution in BFO reduces the leakage current and enhances the ferroelectric switching characteristic while mitigating the stereochemical activity of Bi lone pairs [19]. The reduction in the concentration of charged defects, dielectric loss, or lowering of leakage current achieved by virtue of La doping in BFO are also documented [20,21]. A ferromagnetic behaviour of nanocrystalline Sm doped BFO samples even at room temperature has been observed which is absent in pristine samples, and a few orders of magnitude increase in resistivity are also observed in Sm doped samples. In addition, it has documented a giant change in the magnetodielectric properties of Sm doped samples which plays an important role in the enhancement of multiferroic properties of nanocrystalline Sm doped BFO [22].

It is thus appropriate to choose rare earth ion with a small ionic radius and a high magnetic moment to substitute Bi^{3+} ion equivalently to improve the multiferroic properties of $BiFeO_3$. These improved properties obtained by rare earth doping demonstrate the possibility of enhancing the multiferroic applicability of BFO. On the other hand, with similar electronic structure, especially the lone pair electrons, Pb substitution for Bi is expected to modify the magnetic and ferroelectric properties. Further, the difference in the charge and ionic radii of Bi^{3+} and Pb^{2+} can also direct to topological changes in the oxygen octahedra. One recent study on Pb substitution reported a structural phase transition reducing the rhombohedral distortion and progressively breaking the ferroelectric order [23].

The literature thus witnesses that rare earth elements can improve the ferroelectric and magnetic properties of BFO, but no systematic effort has been made to study the structural, vibrational, and dielectric properties of bulk La and Pb doped $BiFeO_3$ ceramics. With these motivations, we have investigated and compared the crystallographic structure and dielectric properties of pristine $BiFeO_3$ with rare earth (La) doped $BiFeO_3$ ceramics. In order to understand the role of the *R*3*c* to *P4/mmm* structural transition and its associated changes in the vibrational and dielectric behaviour, we have studied the structural, Raman, and dielectric properties of Pb doped $BiFeO_3$ ceramics. The $BiFeO_3$ and $Bi_{0.825}A_{0.175}FeO_3$ (A = La, Pb) ceramics were prepared by solid state reaction route. Characterizations as X-ray diffraction and Raman scattering measurements revealed a consistency of structural properties in La and Pb doped $BiFeO_3$. A detailed structural analysis using the Rietveld refinement method and dielectric properties have been reported.

2 Experimental details

The polycrystalline samples with the compositions $BiFeO_3$ and $Bi_{0.825}A_{0.175}FeO_3$ (A = La, Pb) were prepared by conventional solid state reaction route [24,25]. The starting materials, Bi_2O_3, Fe_2O_3, La_2O_3, and PbO, were weighed, mixed, and grounded thoroughly in an agate mortar and calcined for 6 h at 650 ℃ for the desired composition. All the calcined compositions were uniaxially dye-pressed into pellets with size of 10 mm in diameter and 2 mm in thickness. Sintering was performed at 820 ℃ for 3 h with intermediate grinding. $BiFeO_3$ and $Bi_{0.825}A_{0.175}FeO_3$ (A = La, Pb) were further characterized for structural and electrical properties. Details of the experimental characterization were reported elsewhere [26–29].

The crystal structure and type of phases were identified by means of X-ray powder diffraction (XRPD) at room temperature, using Bruker D8 Advance X-ray diffractometer with Cu $K\alpha_1$ radiation (1.5406 Å) generated at 40 kV and 40 mA power settings. The data were collected at a scanning speed of

2 (°)/min with a step size of 0.02° over the angular range $20° < 2\theta < 80°$. The Raman measurements on synthesized samples were carried out on LABRAM-HR spectrometer with a 488 nm excitation source equipped with a Peltier cooled charge coupled device detector. Frequency dependent dielectric measurements were carried out using an impedance analyzer (Model - Novocontrol tech Germany, alpha ATB) which spans over a wide range of frequency (10 Hz–1 MHz). For dielectric measurements, sintered pellets were polished with zero grain emery paper, and coated with silver paste on adjacent faces as electrodes to make the parallel plate capacitor geometry

3 Results and discussion

3.1 X-ray diffraction

The X-ray diffraction (XRD) patterns of $BiFeO_3$ and $Bi_{0.825}A_{0.175}FeO_3$ (A = La, Pb) ceramic samples are illustrated in Fig. 1. The synthesized ceramic samples are further designated as BFO for $BiFeO_3$, BPFO for $Bi_{0.875}Pb_{0.175}FeO_3$, and BLFO for $Bi_{0.825}La_{0.175}FeO_3$. From the observed XRD patterns, it has been found that the samples exhibit different crystal structures. The XRD pattern of pristine BFO is indexed in the rhombohedral crystal system (space group $R3c$). In BLFO sample, a minor low-intensity impurity peak is detected around $2\theta \approx 27.60°$ associated with $Bi_{25}FeO_{39}$ (shown as # in Fig. 1) [24]. The occurrence of $Bi_{25}FeO_{39}$ secondary phase peaks is generally observed in parent BFO due to the kinetics of phase formation and the high volatility of Bi_2O_3. The diffraction peaks change in both intensity and 2θ value with different doping as a result of change in crystal structure. Pristine $BiFeO_3$ possesses rhombohedral structure with space group $R3c$ and matches well with earlier published reports [19–29].

We may refer to an earlier report on BLFO with a substitutional induced structural phase transition ($R3c \rightarrow C222$) [30]. The XRD pattern of BLFO sample is indexed in rhombohedral ($R3c$) system with lattice parameters $a = b = 5.560(4)$ Å and $c = 13.759(3)$ Å. It reveals that the addition of La does not affect the rhombohedral structure of $BiFeO_3$. Besides, a small shift of the peaks in the lower angle is observed for BLFO relative to BFO. The reflection conditions derived from indexed reflection for BLFO cell are $l = 2n$ for hhl, $k = 2n$ for hkh, $h = 2n$ for hkk, $h = 2n$ for $h00$, $k = 2n$ for $0k0$, and $l = 2n$ for $00l$ which are compatible with $R3c$. Deduced results on BLFO are consistent with the earlier reported work [17].

On Pb doping, the $BiFeO_3$ with rhombohedral structure shows a change to tetragonal (space group $P4/mmm$) as shown in Fig. 1 in the 2θ range of 31°–33°. The two peaks (104) and (110) merged into a single peak at $2\theta = 32°$ in the XRD pattern of BPFO reveal that it possesses a tetragonal structure with space group $P4/mmm$, and a proper coincidence has been found (ICDD) with the pattern powder diffraction format (PDF) No.79-2263. It is clear from the enlarged XRD pattern in the 2θ range of 31°–33° in Fig. 1 that there is a shift of the maximum intense peak with the addition of Pb that corresponds to the BFO phase toward lower angles. So (110) peak corresponds to tetragonal phase of BPFO sample. This means that the addition of the Pb content has led to a structural distortion in the BFO phase [22].

Rietveld refined XRD data plots are shown in Fig. 2. The observations indicate the existence of structural

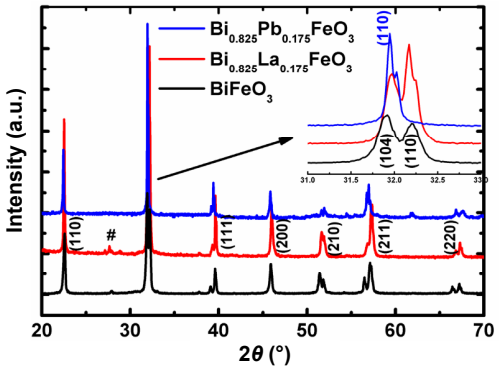

Fig. 1 XRD patterns of the $BiFeO_3$ and $Bi_{0.825}A_{0.175}FeO_3$ (A = La, Pb) samples.

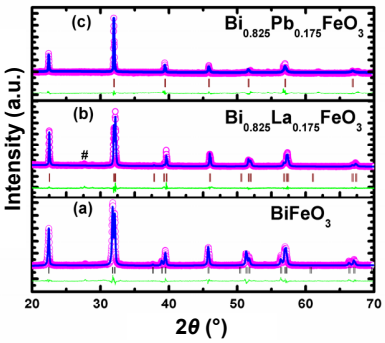

Fig. 2 Rietveld refined XRD patterns of the $BiFeO_3$ and $Bi_{0.825}A_{0.175}FeO_3$ (A = La, Pb) samples. Pink hollow circles represent observed intensity (Y_{obs}), blue solid lines represent calculated intensity (Y_{calc}), green solid lines show the difference in observed and calculated intensities ($Y_{obs}-Y_{calc}$), and peak positions of different phases are shown at the base line as small ticks (|).

transformation with a continual change of structural parameters in the samples with very small rhombohedral distortion. In the tetragonal (space group *P*4/*mmm*) frame of reference, the obtained lattice parameters are $a = 3.9534(4)$ Å, $b = 3.9534(4)$ Å, and $c = 3.9590(4)$ Å for BPFO. We end up by stating that La doping does not show any change in rhombohedral $BiFeO_3$, while Pb doping allows rhombohedral $BiFeO_3$ to tetragonal $Bi_{0.825}Pb_{0.175}FeO_3$ structure. The calculated parameters of parent as well as doped samples after refinement are listed in Table 1. We have illustrated structural parameters for all samples and also identify the residuals for weighted pattern R_{wp}, the expected weighted profile factor R_{exp}, and goodness of fit χ^2.

The stability of perovskite compound based on ABO_3 formula is often discussed in reference to Goldschmidt's tolerance factor *t*. The tolerance factor for $Bi_{0.825}A_{0.175}FeO_3$ (A = La, Pb) can be written as [31]:

$$t = \frac{[(1-x)R_{Bi} + xR_A] + R_O}{\sqrt{2}(R_{Fe} + R_O)} \quad (1)$$

Here, R_{Bi}, R_A, R_{Fe}, and R_O are the effective ionic radii of Bi, *A*, Fe, and O ions, respectively. Based on effective ionic radius values, the tolerance factor *t* for BFO, BLFO, and BPFO is 0.888, 0.879, and 0.891, respectively. It is known that tolerance factor *t* is unity for an ideal perovskite cubic structure. Deduced values of *t* closer to unity infer the stable perovskite phase of BLFO and BPFO.

The crystal structures of $Bi_{0.825}A_{0.175}FeO_3$ (A = La, Pb) samples generated using FullPROF studio program are documented in Fig. 3. It is discerned that BFO possesses a rhombohedrally distorted perovskite with space group *R*3*c*. This structure can be derived from the rotations of the oxygen octahedra around $[111]_c$ direction relative to the parent cubic cell and displacements of the Bi^{3+} and Fe^{3+} cations along the

Table 1 Rietveld refined structural parameters of the BFO, $Bi_{0.825}A_{0.175}FeO_3$ (A = La, Pb) samples simulated based on the measured XRD patterns

Structure	Parameter	Atom	*x*	*y*	*z*	*R* factor (%)
			$BiFeO_3$			
	$a = 5.5798(3)$ Å	Bi	0	0	0.2788	$R_{Bragg} = 3.85$
	$b = 5.5798(3)$ Å	Fe	0	0	0	$R_p = 10.2$
*R*3*c*	$c = 13.867(4)$ Å	O	0.5985	0.7250	0.5714	$R_{wp} = 14.6$
	$V = 373.81(2)$ Å^3					$\chi^2 = 3.76$
	Deviance = 0.920E+04					GoF = 1.9
			$Bi_{0.825}La_{0.175}FeO_3$			
	$a = 5.5604(4)$ Å	Bi/La	0	0	0.2724	$R_{Bragg} = 4.89$
	$b = 5.5604(4)$ Å	Fe	0	0	0	$R_p = 5.36$
*R*3*c*	$c = 13.7596(3)$ Å	O	0.6679	0.7647	0.5489	$R_{wp} = 7.15$
	$V = 368.43(2)$ Å^3					$\chi^2 = 2.91$
	Deviance = 0.883E+04					GoF = 1.7
			$Bi_{0.825}Pb_{0.175}FeO_3$			
	$a = 3.9534(4)$ Å	Bi/Pb	0	0	0	$R_{Bragg} = 10.0$
	$b = 3.9534(4)$ Å	Fe	0.5000	0.5000	0.5000	$R_p = 61.0$
*P*4/*mmm*	$c = 3.9590(4)$ Å	O1	0.5000	0.5000	0	$R_{wp} = 34.8$
	$V = 61.876(2)$ Å^3	O2	0.5000	0	0.5000	$\chi^2 = 3.24$
	Deviance = 0.889E+04					GoF = 1.16

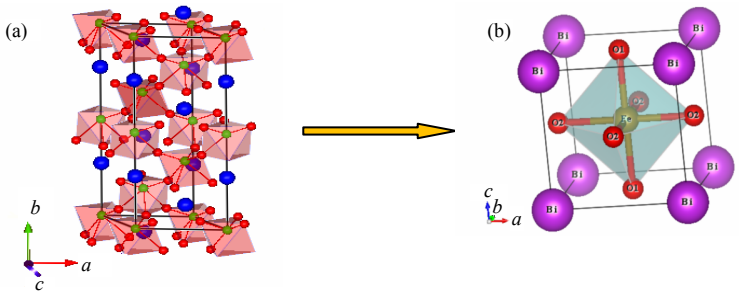

Fig. 3 Schematic representations of the crystal structures expected for $Bi_{0.825}A_{0.175}FeO_3$ (A = La, Pb) compounds with different substituting element: (a) rhombohedral perovskite *R*3*c* structure (representation is based on the refined atomic positions obtained for $Bi_{0.825}La_{0.175}FeO_3$ sample); (b) tetragonal structure *P*4/*mmm* space group (representation is based on the refined atomic positions obtained for $Bi_{0.825}Pb_{0.175}FeO_3$ sample).

same $[111]_c$ direction. Owing to the lone pair effect, the Fe^{3+} ions are in distorted oxygen octahedra, while the Bi^{3+} ions in the dodecahedral positions are strongly shifted from the central position towards one of the Fe^{3+} ions [32,33].

It is now well established that, ferroic order and spontaneous polarization in BFO mainly result from the Bi^{3+} stereochemical $6s^2$ lone pair electrons. Thus, it is expected that, doping of rare earth and metal ion will distort the cation spacing between the oxygen octahedra and alter the long range ferroelectric order. The ferroelectric properties have a close relation with the Fe–O bond length. The interatomic bond lengths with standard deviation of both samples were calculated by using Bond_Str program and are tabulated in Table 2. In BLFO compound with rhombohedral (*R*3*c*) crystal structure, the octahedra bond environment is composed of three long degenerate Fe–O bond lengths and three short degenerate Fe–O bond lengths. On the other hand, the FeO_6 octahedron gets distorted due to Pb substitution, resulting change in bond lengths as illustrated in Table 2.

3. 2 Raman scattering measurements

Figure 4 illustrates the Raman scattering spectra of BFO, BLFO, and BPFO samples with excitation wavelength of 488 nm at room temperature. For rhombohedral structure with space group *R*3*c*, the group theory reveals 13 Raman active modes ($\Gamma_{\text{Raman, }R3c} = 4A_1 + 9E$) and $5A_2$ as Raman inactive modes [34,35]. The selection rule for the Raman active modes for tetragonal structure in polarization configurations with total number of normal Raman modes is $\Gamma_{\text{Raman}} = 4A_1 + B_1 + 4E$ [36,37]. The A_1 modes are associated with Fe ions and *E* modes are associated with Bi ions. The dependence of mode positions on BFO, BLFO, and BPFO samples are shown in Table 3.

Table 2 Important bond lengths of BFO and $Bi_{0.825}A_{0.175}FeO_3$ (*A* = La, Pb) samples

Compound	Bond type	Bond length (Å)	Deviation
BFO	Bi–O	2.231	0.204
	Bi–O	2.538	
	Fe–O	1.784	
	Fe–O	2.330	
BLFO	Bi/La–O	2.784	0.168
	Bi/La–O	2.791	
	Fe–O(3)	1.777	
	Fe–O(3)	2.231	
BPFO	Bi/Pb–O1	2.793	0.147
	Bi/Pb–O2	2.795	
	Fe–O1	1.978	
	Fe–O2	1.975	

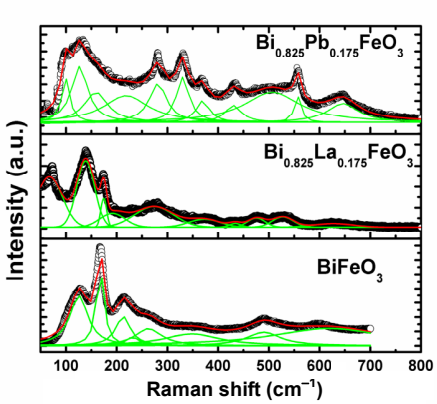

Fig. 4 Room temperature Raman spectra for $BiFeO_3$ and $Bi_{0.825}A_{0.175}FeO_3$ (*A* = La, Pb) samples.

In BFO, all phonon modes are polar, which means that they are oblique when measured in arbitrary directions. The only possibility of simple comparison would be possible with oriented single crystal in special geometries. Otherwise, it is very difficult to compare spectra of different samples and even of the same sample in different positions (ceramics, polycrystals) or orientations (single crystals). We have found that the first three strong peaks at 126, 167, and 217 cm^{-1} manifest A_1-1, A_1-2, and A_1-3 modes respectively, even though A_1-4 at 425 cm^{-1} is completely decomposed in parent BFO. Moreover, rest of the obtained modes at 259, 280, 327, 365, 490, and 597 cm^{-1} are assigned as *E*-3, *E*-4, *E*-5, *E*-6, *E*-7, and *E*-9, respectively [13,14].

In the present study, ten Raman active phonon modes of BLFO sample including A_1-1, A_1-2, A_1-4, *E*-1, *E*-4, *E*-6, *E*-7, *E*-8, and *E*-9 modes at 135.95, 174.52, 434.14, 67.44, 273.93, 373.35, 475.53, 527.78, and

Table 3 Raman modes for $BiFeO_3$, $Bi_{0.825}A_{0.175}FeO_3$ (*A* = La, Pb) samples, and the bulk $BiFeO_3$ (Kothari *et al.* [38]) (Unit: cm^{-1})

Raman mode	BFO bulk [38]	BFO	BLFO	BPFO
A_1-1	135.15	126	135	127
A_1-2	167.08	167	174	159
A_1-3	218.11	217	—	—
A_1-4	430.95	—	434	429
E-1	71.39	—	68	63
E-2	98.36	—	—	—
E-3	255.38	259	—	218
E-4	283.0	280	274	281
E-5	321.47	327	—	330
E-6	351.55	365	373	369
E-7	467.60	490	476	506
E-8	526.22	—	528	556
E-9	598.84	597	628	646

627.47 cm^{-1} match well with earlier reported bulk BFO sample [38]. The ferroelectricity of BFO generally originates from the stereochemical activity of the Bi^{3+} $6s^2$ lone pair electrons that are mainly responsible for the change in both Bi–O covalent bonds. The six characteristic modes, i.e., *E*-1, A_1-1, A_1-2, A_1-3, A_1-4, and *E*-2 are believed to be responsible for the ferroelectric nature of the bismuth ferrite samples.

As evident from the XRD, the crystal symmetry varies from rhombohedral (BLFO) to tetragonal (BPFO) structure. These changes in crystal structure are attributed to the *A*-site disorder created by (La and Pb) substitution, which leads to the shifting of Raman modes with sudden disappearance of some modes. The normal modes related to the Bi–O covalent bonds (i.e., *E*-1, A_1-1, A_1-2, A_1-3, and *E*-2 modes) shift gradually towards higher frequencies and are attributed to the substitution of (mass) La (138.90 g) ion for Bi (208.98 g) ion in the $BiFeO_3$, while the same modes shift towards lower frequencies for relatively equal atomic mass of Pb (207.2 g) ion for Bi (208.98 g) ion in the $BiFeO_3$. Henceforth, shifting depends on the atomic mass of the dopants.

3. 3 Dielectric measurements

At room temperature, the frequency dependence of dielectric constant (ε') and dielectric loss ($\tan\delta$) of BLFO and BPFO ceramics are illustrated in Fig. 5, and ε' and $\tan\delta$ of BFO ceramics are shown in the insets of Fig. 5. For both doped samples, ε' gradually decreases with increasing frequency at low frequencies and remains fairly constant at higher frequencies. The low frequency dispersion can be attributed to Maxwell–Wagner type interfacial polarization. These dipoles may arise due to charge defects (V_{Bi}^{3-} , V_O^{2+}) and localized charges [39]. Similar trend has earlier been reported in Dy^{3+}, Sm^{3+}, and La^{3+} doped BFO ceramics [30,40–42] and Ho doped $YmnO_3$ [43]. The corresponding values of ε' at 100 Hz for the BFO, BLFO, and BPFO ceramics are about 135, 21, and 42, respectively. At higher frequencies, charge dipoles do not have adequate time to follow the applied field and undergo relaxation.

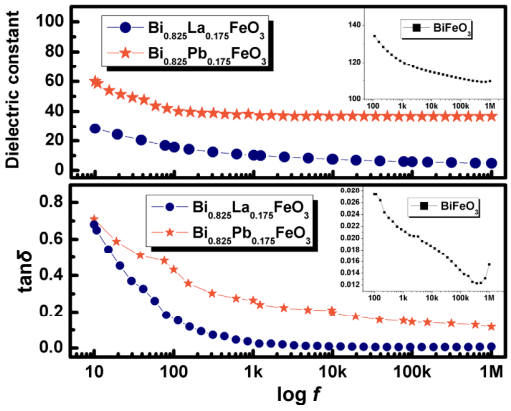

Fig. 5 Room temperature dielectric constant and dielectric loss for $Bi_{0.825}A_{0.175}FeO_3$ (*A* = La, Pb) samples. Insets show the dielectric constant and loss for $BiFeO_3$.

At sufficiently low frequency, charged defects (V_O^{2+} , V_{Bi}^{3-} , and Fe^{2+}) are able to follow the applied electric field, resulting in increased ε' and $\tan\delta$ values. The weak dependence of ε' and $\tan\delta$ on frequency along with the generally low $\tan\delta$ values is seen for BLFO and BPFO at higher frequencies. We may comment that electrons/domains rather than dipoles of the charged defects mainly contribute to the characteristics of ε' and $\tan\delta$ for higher frequency region. For BLFO, this low frequency dispersion and the value of $\tan\delta$ are reduced exhibiting reduced conductivity.

4 Conclusions

In summary, polycrystalline samples of $BiFeO_3$ and $Bi_{0.825}A_{0.175}FeO_3$ (*A* = La, Pb) were successfully prepared by solid state reaction route. The motivation was to probe possible structural change and a comparison of rare earth and metal ion doping in pristine $BiFeO_3$. X-ray powder diffraction and Raman scattering measurements were used to probe the structural changes, if any. The XRD data of as prepared samples were fitted with Rietveld refinement using FullPROF program. BFO and BLFO (La doped $BiFeO_3$) crystallized in rhombohedral structure (*R*3*c*), whereas BPFO (Pb doped $BiFeO_3$) showed tetragonal structure (*P*4/*mmm*).

The change in the crystal symmetry was also confirmed by Raman scattering measurements. The ferroelectricity of BFO generally originates from the stereochemical activity of the Bi^{3+} $6s^2$ lone pair electrons that are mainly responsible for the change in both Bi–O covalent bonds. The six characteristic modes, i.e., *E*-1, A_1-1, A_1-2, A_1-3, A_1-4, and *E*-2 are believed to be responsible for the ferroelectric nature of the bismuth ferrite samples. The change in crystal structure was attributed to the *A*-site disorder created by rare earth and metal ion substitution, which leads to

the shifting of Raman modes with sudden disappearance of some modes. From the frequency dependent dielectric constant and dielectric loss plots, a decrease in dielectric values with increase in frequency is observed for both La and Pb doped samples and can be understand by Maxwell–Wagner type interfacial polarization. BPFO documents larger dielectric constant as compared to BLFO at all frequencies. Porous ceramics with lower value of dielectric constant are most useful for microelectronics. Further studies are still needed to carefully complement the magnetic and electric properties after La/Pb substitution in BFO.

Acknowledgements

UGC-DAE-CSR as an institute is acknowledged for extending its facilities and financial assistance. Authors are thankful to Dr. M. Gupta and Dr. V. Sathe of UGC-DAE-CSR, Indore, for useful discussions.

References

[1] Fiebig M. Revival of the magnetoelectric effect. *J Phys D: Appl Phys* 2005, **38**: R123.

[2] Catalan G, Scott JF. Physics and applications of bismuth ferrite. *Adv Mater* 2009, **21**: 2463–2485.

[3] Neaton JB, Ederer C, Waghmare UV, *et al*. First-principles study of spontaneous polarization in multiferroic $BiFeO_3$. *Phys Rev B* 2005, **71**: 014113.

[4] Sosnowska I, Neumair TP, Steichele E. Spiral magnetic ordering in bismuth ferrite. *J Phys C: Solid State Phys* 1982, **15**: 4835.

[5] Kaczmarek W, Pajak Z, Połomska M. Differential thermal analysis of phase transitions in $(Bi_{1-x}La_x)FeO_3$ solid solution. *Solid State Commun* 1975, **17**: 807–810.

[6] Mukherjee A, Basu S, Chakraborty G, *et al*. Effect of Y-doping on the electrical transport properties of nanocrystalline $BiFeO_3$. *J Appl Phys* 2012, **112**: 014321.

[7] Zalesskii AV, Frolov AA, Khimich TA, *et al*. Composition-induced transition of spin-modulated structure into a uniform antiferromagnetic state in a $Bi_{1-x}La_xFeO_3$ system studied using ^{57}Fe NMR. *Phys Solid State+* 2003, **45**: 141–145.

[8] Palkar VR, Kundaliya DC, Malik SK, *et al*. Magnetoelectricity at room temperature in the $Bi_{0.9-x}Tb_xLa_{0.1}FeO_3$ system. *Phys Rev B* 2004, **69**: 212102.

[9] Cheng ZX, Li AH, Wang XL, *et al*. Structure, ferroelectric properties, and magnetic properties of the La-doped bismuth ferrite. *J Appl Phys* 2008, **103**: 07E507.

[10] Le Bras G, Colson D, Forget A, *et al*. Magnetization and magnetoelectric effect in $Bi_{1-x}La_xFeO_3$ ($0 \leqslant x \leqslant 0.15$). *Phys Rev B* 2009, **80**: 134417.

[11] Zhang S-T, Zhang Y, Lu M-H, *et al*. Substitution-induced phase transition and enhanced multiferroic properties of $Bi_{1-x}La_xFeO_3$ ceramics. *Appl Phys Lett* 2006, **88**: 162901.

[12] Yuan GL, Or SW, Liu JM, *et al*. Structural transformation and ferroelectromagnetic behavior in single-phase $Bi_{1-x}Nd_xFeO_3$ multiferroic ceramics. *Appl Phys Lett* 2006, **89**: 052905.

[13] Yuan GL, Or SW. Enhanced piezoelectric and pyroelectric effects in single-phase multiferroic $Bi_{1-x}Nd_xFeO_3$ (x = 0–0.15) ceramics. *Appl Phys Lett* 2006, **88**: 062905.

[14] Yuan GL, Or SW, Chan HLW. Structural transformation and ferroelectric–paraelectric phase transition in $Bi_{1-x}La_xFeO_3$ (x = 0–0.25) multiferroic ceramics. *J Phys D: Appl Phys* 2009, **40**: 1196.

[15] Khomchenko VA, Kiselev DA, Bdikin IK, *et al*. Crystal structure and multiferroic properties of Gd-substituted $BiFeO_3$. *Appl Phys Lett* 2008, **93**: 262905.

[16] Mukherjee A, Basu S, Manna PK, *et al*. Enhancement of multiferroic properties of nanocrystalline $BiFeO_3$ powder by Gd-doping. *J Alloys Compd* 2014, **598**: 142–150.

[17] Khomchenko VA, Karpinsky DV, Kholkin AL, *et al*. Rhombohedral-to-orthorhombic transition and multiferroic properties of Dy-substituted $BiFeO_3$. *J Appl Phys* 2010, **108**: 074109.

[18] Qian FZ, Jiang JS, Jiang DM, *et al*. Multiferroic properties of $Bi_{0.8}Dy_{0.2-x}La_xFeO_3$ nanoparticles. *J Phys D: Appl Phys* 2010, **43**: 025403.

[19] Jeon N, Rout D, Kim IW, *et al*. Enhanced multiferroic properties of single-phase $BiFeO_3$ bulk ceramics by Ho doping. *Appl Phys Lett* 2011, **98**: 072901.

[20] Hossain SKM, Mukherjee A, Chakraborty S, *et al*. Enhanced multiferroic properties of nanocrystalline La-doped $BiFeO_3$. *Materials Focus* 2013, **2**: 92–98.

[21] Wang Y, Zheng RY, Sim CH, *et al*. Charged defects and their effects on electrical behavior in $Bi_{1-x}La_xFeO_3$ thin films. *J Appl Phys* 2009, **105**: 016106.

[22] Mukherjee A, Basu S, Manna PK, *et al*. Giant magnetodielectric and enhanced multiferroic properties of Sm doped bismuth ferrite nanoparticles. *J Mater Chem C* 2014, **2**: 5885–5891.

[23] Chaigneau J, Haumont R, Kiat JM. Ferroelectric order stability in the $Bi_{1-x}Pb_xFeO_3$ solid solution. *Phys Rev B* 2009, **80**: 184107.

[24] Sharma P, Varshney D. Effect of La and Pb substitution on structural and electrical properties of parent and La/Pb co doped $BiFeO_3$ multiferroic. *Adv Mater Lett* 2014, **5**: 71–74.

[25] Sharma P, Satapathy S, Varshney D, *et al*. Effect of sintering temperature on structure and multiferroic properties of $Bi_{0.825}Sm_{0.175}FeO_3$ ceramics. *Mater Chem Phys* 2015, **162**: 469–476.

[26] Varshney D, Kumar A, Verma K. Effect of A site and B site doping on structural, thermal, and dielectric properties of $BiFeO_3$ ceramics. *J Alloys Compd* 2011, **509**: 8421–8426.

[27] Varshney D, Kumar A. Structural, Raman and dielectric behavior in $Bi_{1-x}Sr_xFeO_3$ multiferroic. *J Mol Struct* 2013, **1038**: 242–249.

[28] Sharma P, Varshney D, Satapathy S, *et al*. Effect of Pr substitution on structural and electrical properties of $BiFeO_3$ ceramics. *Mater Chem Phys* 2014, **143**: 629–636.

[29] Kumar A, Varshney D. Crystal structure refinement of $Bi_{1-x}Nd_xFeO_3$ multiferroic by the Rietveld method. *Ceram Int* 2012, **38**: 3935–3942.

[30] Jiang Q-H, Nan C-W, Shen Z-J. Synthesis and properties of multiferroic La-modified $BiFeO_3$ ceramics. *J Am Ceram Soc* 2006, **89**: 2123–2127.

[31] Goldschmidt VM. Die Gesetze der Krystallochemie. *Naturwissenschaften* 1926, **14**: 477–485.

[32] Fischer P, Polomskya M, Sosnowska I, *et al*. Temperature dependence of the crystal and magnetic structures of $BiFeO_3$. *J Phys C: Solid State Phys* 1980, **13**: 1931.

[33] Bucci JD, Robertson BK, James WJ. The precision determination of the lattice parameters and the coefficients of thermal expansion of $BiFeO_3$. *J Appl Cryst* 1972, **5**: 187–191.

[34] Singh MK, Jang HM, Ryu S, *et al*. Polarized Raman scattering of multiferroic $BiFeO_3$ epitaxial films with rhombohedral *R*3*c* symmetry. *Appl Phys Lett* 2006, **88**: 42907.

[35] Haumont R, Kreisel J, Bouvier P, *et al*. Phonon anomalies and the ferroelectric phase transition in multiferroic $BiFeO_3$. *Phys Rev B* 2006, **73**: 132101.

[36] Varshney D, Sharma P, Satapathy S, *et al*. Structural, electrical and magnetic properties of $Bi_{0.825}Pb_{0.175}FeO_3$, and $Bi_{0.725}La_{0.1}Pb_{0.175}FeO_3$ multiferroics. *Mater Res Bull* 2014, **49**: 345–351.

[37] Varshney D, Sharma P, Satapathy S, *et al*. Structural, magnetic and dielectric properties of Pr-modified $BiFeO_3$ multiferroic. *J Alloys Compd* 2014 **584**: 232–239.

[38] Kothari D, Reddy VR, Sathe VG, *et al*. Raman scattering study of polycrystalline magnetoelectric $BiFeO_3$. *J Magn Magn Mater* 2008, **320**: 548–552.

[39] Chakrabarti K, Das K, Sarkar B, *et al*. Enhanced magnetic and dielectric properties of Eu and Co co-doped $BiFeO_3$ nanoparticles. *Appl Phys Lett* 2012, **101**: 042401.

[40] Uniyal P, Yadav KL. Observation of the room temperature magnetoelectric effect in Dy doped $BiFeO_3$. *J Phys: Condens Matter* 2009, **21**: 012205.

[41] Yuan GL, Or SW. Multiferroicity in polarized single-phase $Bi_{0.875}Sm_{0.125}FeO_3$ ceramics. *J Appl Phys* 2006, **100**: 024109.

[42] Sharma P, Kumar A, Varshney D. Enhanced magnetic response in single-phase $Bi_{0.80}La_{0.15}A_{0.05}FeO_{3-\delta}$ (A = Ca, Sr, Ba) ceramics. *Solid State Commun* 2015, **220**: 6–11.

[43] Varshney D, Sharma P, Kumar A. Room temperature structure vibrational and dielectric properties of Ho modified $YMnO_3$. *Mater Res Express* 2015, **2**: 076102.